The International Archives of the Photogrammetry, Remote Sensing and Spatial Information Sciences, Volume XLVIII-M-9-2025
30th CIPA Symposium “Heritage Conservation from Bits:
From Digital Documentation to Data-driven Heritage Conservation”, 25–29 August 2025, Seoul, Republic of Korea

# Photogrammetric Localisation of Electromagnetic Sensors for Detecting Anomalies in Heritage Internal Wood Structures

Maria Chizhova[1]*, Jakub Markiewicz[2], Patryk Kot[3], Thomas Eißing[1]

[1] Centre for Heritage Conservation Studies and Technologies (KDWT), University of Bamberg, Germany - (maria.chizhova, thomas.eissing)@uni-bamberg.de
[2] Faculty of Geodesy and Cartography, Warsaw University of Technology, Poland - jakub.markiewicz@pw.edu.pl
[3] Infection Innovation Technology Laboratory (iiTECH), Infection Innovation Consortium (iiCON), Liverpool School of Tropical Medicine, UK - patryk.Kot@lstmed.ac.uk

**Keywords:** Data Fusion, Electromagnetic Sensor, Monitoring, Optical Imaging, Timber Stability.

**Abstract**

The strength estimation of built-in historical timber requires extensive investigation of internal wooden structures and properties, which cannot be mapped using only optical surveying methods. In most cases, additional equipment is required, including invasive techniques such as drilling resistance technology and sensitive methods such as ultrasonics or electromagnetic (EM) sensor technology. Thus, the localisation of a measuring device within a whole timber structure and the uniform registration of internal and external wooden structures is missing. In this article, we investigate the capability to localise the EM sensor, which will be used in future research activities for in-depth analysis of internal timber structures. The position of the EM sensor will be captured during the 3D timber imaging using different optical methods to provide a reference between the external wood surface and digitised internal structures. The data quality is compared and evaluated according to the measurement method using geometric features and visual expertise.

## 1. Introduction

### 1.1 Problem statement

Wood strength, i.e. its resistance to breakage, is fundamental for the structural analysis of historic timber constructions. The exact strength values of historic timbers are generally unknown. Consequently, for safety reasons, the lowest values are usually assumed (this also means the lowest quality and grade class), although the actual strength values could be higher. This removes and replaces larger quantities of heritage timbers than is technically necessary. There are several methods to estimate the timber's strength directly using instrumental inspection (e.g. drilling, ultrasonic techniques), as well as indirectly from certain visual features (e.g. wood knots, cracks, insect infestation) (Ebner, 2018; Erler, 2004; Linke, 2024; Linke et al., 2017).

The most accurate and objective methods are resistance techniques (Rinn, 2016; Rug and Held, 1995), which allow moisture content estimation in timber and localisation of internal defects indicating the relative timber strength (Fig. 1).

A drilling needle is driven into the wood at a constant feed rate during drilling resistance measurement (Fig. 1a). Drilling resistance is provided as a digital curve, characterised by various factors such as raw density, wood moisture and wood damages like cracks, insect affection and knots (Fig. 1b).

To quantify wood moisture, insulated measuring tips are driven into the depth of the wood to measure the resistance between two electrodes by adjusting the type of wood and temperature. The wood moisture is measured in mass per cent, or M-% for short, and a resistance-wood moisture characteristic curve is interpolated from the measured values (Fig. 1 c,d). However, both methods are invasive procedures generally less appropriate for cultural heritage analyses. Impulse tomography is a non-invasive method whereby tomograms (virtual slices) are created through the wood to detect internal damage that affects timber strength (Hasenstab, 2005).

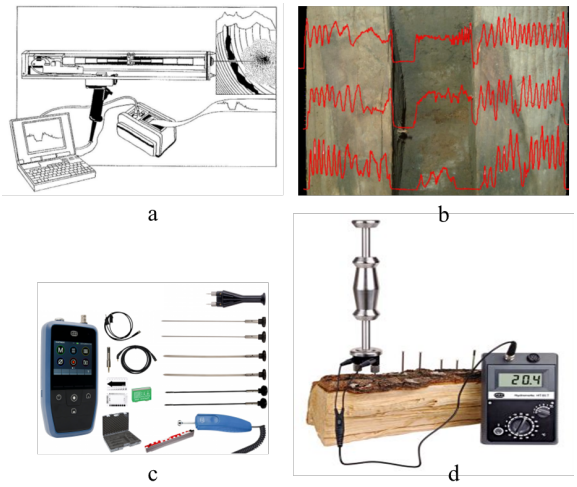


Figure 1. Invasive methods for investigation of internal wooden structure: (a,b) drilling resistance technique with the resulting curve (Ebner, 2018; Rinn, 2016) and (c,d) moisture analysis device (Gann product images).

The sensors are placed around the beam (Fig. 2b), which is relatively complicated in roof structures where the individual beams are inaccessible from all sides. Computer tomography is also used to analyse internal wood structures, which can be used for newly manufactured, not built-in beams (Fig. 2a).

Investigation and visualisation of internal wood structures (crack depth, insect holes, moisture) is a particular challenge for heritage timber constructions since i) invasive methods should be used to a very limited extent in comparison to new wood, and ii) the wooden timbers would not be removed from the

building for investigation using precise active measurement methods such as computer tomography.

a b

Figure 2. The example of (a) CT.LOG computer tomograph (Hansmann et al., 2018) and (b) ARBOTOM impulse tomograph from RINNTECH (Ebner, 2018).

Electromagnetic (EM) spectroscopy has gained considerable interest in recent years as a promising method for structural analysis in various fields, especially civil engineering (Kot et al., 2021). The technique has been successfully used as a non-contact technique (Kot et al., 2016; Muradov et al., 2022) and an embedded system for long-term monitoring (Gkantou et al., 2019). In our further study, we want to explore the possibilities of using EM technology to detect and analyse internal wooden structures and the characteristics of historically built-in timbers. In contrast to other methods, this technology is entirely non-invasive, fast and more accessible to handle (Fig. 3).

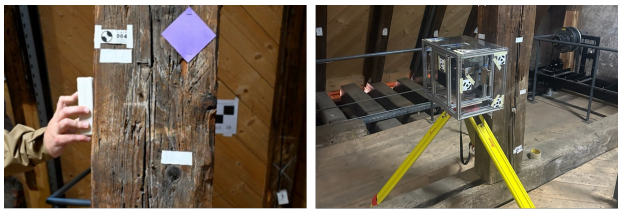

a b

Figure 3. Different types of EM sensors.

### 1.2 Different Geolocalisation Methods and 3D Shape

One of the critical elements related to the acquisition and processing of EM sensors-derived data is georeferencing, aimed at spatially orientating the sensor in the adopted reference system. Many approaches and methods are based on different sensors and approaches to determine direct georeferenced (Markiewicz et al., 2020).

Indoor Positioning Systems (IPS) deliver precise localisation in environments where Global Navigation Satellite Systems (GNSS) are ineffective (Puertolas-Montañez et al., 2013), employing technologies like Radio Frequency (RF), ultrasound, infrared (IR), and optical systems. RF methods, such as Bluetooth Low Energy (BLE), Ultra-wideband (UWB), and Radio-Frequency Identification (RFID), achieve accuracies ranging from meters (BLE, WLAN) to centimetres (RFID) (Amsters et al., 2019; Xu et al., 2018; Zafari et al., 2017). Ultrasound systems like Cricket and Dolphin offer high accuracy but are influenced by environmental factors like humidity and temperature (Ijaz et al., 2013; Li et al., 2016). IR systems, while cost-effective, require unobstructed line-of-sight and provide accuracies from meters to submillimetres, depending on the sensor type (Mautz, 2012). Optical techniques, including visual markers and Simultaneous Localisation and Mapping (SLAM), use camera data for localisation, with applications ranging from 3D mapping to dense point cloud generation (Bianco et al., 2018). Terrestrial Laser Scanning (TLS) and Close-Range Photogrammetry enhance IPS by providing high-resolution 3D data with millimetre to submillimetre precision. However, TLS accuracy is affected by surface reflectivity and environmental conditions (Kersten and Lindstaedt, 2022; Li et al., 2018; Medic et al., 2019; Tan and Cheng, 2016). At the same time, photogrammetry relies on algorithms like Structure-from-Motion (SfM) and Multi-View Stereo (MVS) for accurate image-based reconstructions (Bianco et al., 2018; Nyimbili et al., 2016). These technologies, alongside classical surveying techniques like tachometer and geodetic network adjustments, offer comprehensive localisation solutions, with methods like the Gauss-Markov model ensuring robust error analysis and accuracy verification (Börlin et al., 2018; Teunissen, 2024).

When analysing complex structures, a device must match a wooden surface's internal and external characteristics and properly localise detected features within the timber. This is crucial for correctly processing electromagnetic sensor data, as it affects the correctness of signal correction and the prediction of damage occurring inside and outside the analysed timbers.

The first research on selecting the appropriate evaluation and orientation accuracy of the EM sensors was presented in the article "The Quality Assessment of Different Geolocalisation Methods for a Sensor System to Monitor Structural Health of Monumental Objects" (Markiewicz et al., 2020). From the results presented there, it appeared that the use of photogrammetric methods based on close-range images gave a recommended accuracy of orientation for the 'large system' of electromagnetic sensors (Fig. 4a). The research presented in this article is a continuation of research into the selection of data registration methods. In contrast to previous investigations, the oriented system is much smaller (which affected the image acquisition and processing). Additionally, as part of this research, it was decided to evaluate the selection of the method for generating dense point clouds used for EM sensor orientation, signal enhancement and correction, and face timber analyses.

This article investigates the possibilities of localising the EM sensor using a photogrammetric approach. Thus, a photogrammetric approach to create a 3D model that represents the position of the EM sensor within the timber will be investigated using different matching and data recording techniques. The most successful method will be identified by analysing geometrical features and visually evaluating resulting 3D point clouds. Additionally, the photogrammetry data will be compared with terrestrial laser scanning data.

## 2. Materials and Methods

### 2.1 Case study

The roof construction of the Dominican Church in Bamberg (Germany) has been selected as a research object for investigating historic timbers. The roof structure is around 600 years old. It contains timbers dated from the 12th century onwards, the subject of study at the Centre for Heritage Conservation Studies and Technologies (KDWT) at Bamberg University (Research Lab for Dendrochronology and Structure). The study was initially carried out on four load-bearing timbers in the choir section, demonstrating cracks in varying depths and sizes, knottiness and wood surface defects.

Individual points along the beams were marked to indicate areas for sensor recording (Fig. 4a). Terrestrial laser scanning of the choir area containing these timbers has been conducted to define rough spatial positioning (Fig. 4b).

The entire scene, as well as the individual beams, were investigated using

- close-range images (Nikon D3400 with 18-55 lens)
- iPhone 3dScannerApp (mode "Photogrammetry", optimised by LiDAR)
- Terrestrial laser scanning (Leica BLK360, the highest quality with images (HDR)).

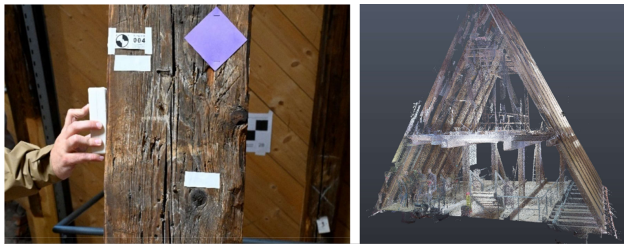

a b

Figure 4. (a) EM sensor recording, and (b) 3D point cloud of the region containing timbers selected for investigation.

### 2.2 Data registration workflow

The proposed geolocalisation method for the sensor system employs a multi-stage process that integrates widely used algorithms implemented in Agisoft Metashape with custom software and open-source libraries such as Open3D (Open3D, 2024) and NumPy (NumPy, 2024). Open3D facilitates 3D data processing, visualisation, and analysis, while NumPy is used for efficient numerical computations, such as matrix operations and linear algebra, which are crucial for geospatial transformations and sensor calibration. This combination enables the seamless integration of photogrammetric and computational methods to achieve accurate and efficient geolocalisation results.

The proposed sensor registration method is a novel approach for determining the exterior orientation parameters, specifically, the X, Y, and Z-coordinates of the antenna centre and the three angular parameters (ω,ϕ,κ) of the electromagnetic (EM) sensor, as well as its relative orientation parameters concerning a reference plane, termed the "base plane," which corresponds to the examined wall and serves as the measurement subject of the EM sensor. This dual-stage calculation of orientation parameters enables accurate determination of the sensor's spatial position while providing critical input for electromagnetic data processing. These parameters serve as the foundation for computing corrections to be applied to the raw data collected by the sensor, thereby enhancing the precision and reliability of the resultant measurements.

The whole data processing workflow was divided into four main parts:

**2.2.1 Determination of the reference system and base planes (data pre-processing):** The reference system was defined at this stage, and the data designated as the basis for subsequent analyses were identified. The commonly used SfM method for orienting close-range images was used at this stage. The images were orientated concerning each other, away from the individual timbers, and fed into an external reference system based on the reference control points. This ensured that each timber was georeferenced to an external reference system. This process was carried out using Agisoft Metashape software. The processing of the data produced internal and external orientation elements for the images, making their further use possible in subsequent stages of EM sensor georeferencing. In addition, the images were grouped and assigned to individual timbers.

**2.2.2 The sensor's images orientation relates to base plane images:** The following data processing stage involved orientating the images showing the EM sensor relative to the images showing the individual timbers. This scenario utilised a feature-based orientation approach implemented in Agisoft Metashape software.

In the initial phase, images capturing the wall were aligned using control and check points acquired through total station measurements, establishing a reference dataset for subsequent processing. The following step involved determining the relative orientation of the images acquired at each sensor station to ensure spatial consistency across the dataset. In addition, coded points were distributed on the device to show off the relative orientation images representing the EM sensors (Fig. 5).

Figure 5. Examples of circular coded targets on the sensor case

**2.2.3 Dense point cloud generation:** The OpenMVS 2.0 library was chosen to generate dense point clouds, as it allows complete customisation and selection of parameters for the generated point clouds (unlike the proprietary solution implemented in Agisoft Metashape). Additionally, the choice of this solution was influenced by the possibility of testing two widely used methods for 3D shape reconstruction, namely Patch-based Multi-View Stereo and Semi-Global Matching. Table 1 provides a list of parameters used for generating dense point clouds.

The selection of parameters, including image resolution, number of views (nearest neighbour images) used for depth-map estimation, iterations (number of patch-match iterations), and geometric iterations (number of geometric consistent iterations), enabled an analysis of the impact of these factors on the accuracy of 3D shape reconstruction based on close-range. and geometric iterations (number of geometric consistent iterations) enabled an analysis of the impact of these factors on the accuracy of 3D shape reconstruction based on close-range images. The iPhone-based recording was carried out using 3dScannerApp in photogrammetric mode and optimised by LiDAR. The 3D timber models have been created with approx. 120-140 images per each beam. For the terrestrial laser scanning, we used the highest resolution and HDR image capturing mode for point cloud colourisation.

**2.2.4 Sensor orientation**

The algorithm for determining sensor orientation was developed using the Open3D library and NumPy capabilities. The process of determining the position and orientation of the EM sensor relative to the reference timber face consisted of the following steps:

| Timber sample | Quality Parameter (Image resolution) | Filtering mode | Number of Views | Fusion mode | Number of iterations | Number of iterations |
|---|---|---|---|---|---|---|
| PBM1 | 1<br>½ of the original image resolution | 0<br>(no-filtering/ raw data) | 4 | 0 | 10 | 10 |
| PBM2 | | | 3 | | | |
| PBM3 | | | 2 | | | |
| PBM4 | | | 5 | | | |
| PBM5 | | | 6 | | | |
| PBM6 | | | 6 | | | |
| PBM7 | | | 8 | | | |
| SGM1 | | | 8 | -1<br>-2 | | |
| SGM2 | | | 6 | | | |
| SGM3 | | | 5 | | | |
| SGM4 | | | 4 | | | |
| SGM5 | | | 3 | | | |
| SGM6 | | | 2 | | | |

Table 1. The list of Parameters Used for Generating Dense Point Clouds in OpenMVS 2.0

**Point Cloud Loading**: The "reference" point cloud and the "point cloud with the EM sensor" were loaded.
**Target Identification**: Based on the XYZ coordinates of circle-coded targets (Fig. 6b), points were identified within a sphere of a 5 cm radius using the KNN search algorithm.
**Plane Fitting**: A plane was fitted to the points identified in Step 2, determining a normal vector and defining a bounding box.
**Projection:** Using the XYZ coordinates of the circle-coded targets and the normal vector of the plane determined in Step 3, the points were projected along the normal vector onto the reference point cloud.
**Local Plane Refinement**: Points within a 1 cm radius of the projected points from Step 4 were identified, and a new plane with its normal vector was fitted.
**Angle Calculation**: The angle between the normal vectors of the planes determined in steps 3 and 5 was calculated, followed by decomposition into principal components.
**Position Determination**: The centroid of the bounding box determined in Step 3 and the angles calculated in Step 6 enabled the determination of the EM sensor's position relative to the reference timber face.

### 2.3 Quality assessment techniques

The accuracy of shape representation and point clouds analysis were assessed based on visual evaluation (e.g., identification of visible outliers and noise). Additionally, the following geometric features were analysed (Table 3):
**Planarity**: since timbers form a cuboid, the planarity of timber sides was estimated by fitting a plane to the timber point cloud and measuring the deviation of the points from this plane. Generally, high planarity indicates a consistent surface, which may be desirable for manufacturing, such as newly produced wood beams. In CloudCompare, the planarity estimation of a point cloud is typically a unitless value ranging from 0 to 1 (highly planar surface). Planarity allows the detection of these features in the case of heritage timbers containing geometric characteristics like cracks or processing traces. In this context, high uniformly distributed planarity may indicate that the data is strongly blurred and, therefore, not accurate enough.
**Normal change rate (NCR)**: a similar task estimates a normal change rate, which examines the variation of normals calculated at each point in the cloud using the angle between normals in neighbouring points. The NCR units are expressed in degrees (°) or radians (rad), intrinsically related to angular measurements. A lower NCR indicates a smoother surface, whereas a higher rate implies greater variations in surface orientation. Significant changes in the normal direction can indicate edges resulting from cracks and processing marks on wood, timber corners, and noise within the data. Even in this case, heritage wooden surfaces are not expected to be highly uniform.
**Roughness**: this parameter measures the variations in the height of points on a surface and gives insight into the spatial frequency distribution of points in the cloud and noise. In our case, high roughness may indicate noise or point cloud artefacts. Roughness is typically measured in terms of the standard deviation of point heights in the local neighbourhood of a point. This is usually expressed in the same units as the coordinate values of the point cloud, such as meters or centimetres, depending on the scale of the dataset.
**Statistical outliers**: for better reliability and confidence in the data consistency, the point cloud has been analysed in terms of outliers, which could be detected visually (e.g., artefacts on corners) and statistically using statistical outlier removal (SOR) or clustering approaches to filter outliers in a point cloud. The values are typically unitless, as they often involve a ratio type of measure (in our case, the number of standard deviations from the mean).
**Surface density**: surface density is also essential, reflecting the spatial information captured. It is generally measured in points per unit area (pts/m2). This metric indicates how many points are present within a defined area on the surface of the point cloud. A correspondingly higher surface density is expected for reliable reconstruction results and accurate correlation between internal and external wood structures.

| Timber | Number of images | Number of tie points | Number of control/check points | RMSE reprojection error [pix] | RMSE on control points [mm] | | | RMSE on check points [mm] | | |
|---|---|---|---|---|---|---|---|---|---|---|
| | | | | | X | Y | Z | X | Y | Z |
| 1 | 65 | 131.130 | 14 | 1.6 | 7.7 | 2.6 | 2.3 | 5.7 | 7.2 | 3.6 |
| 2 | 68 | 227.959 | 7 | 1.6 | 3.6 | 5.1 | 2.0 | 11.3 | 5.0 | 2.2 |
| 3 | 86 | 151.491 | 11 | 1.7 | 4.3 | 5.2 | 1.1 | 4.7 | 2.5 | 3.0 |
| 4 | 71 | 111.863 | 24 | 1.3 | 3.2 | 2.2 | 2.7 | 13.2 | 12.9 | 6.5 |

Table 2. The statistical analysis of the quality assessment of image orientation was used to reference timber system determination and sensor positions.

## 3. Results

### 3.1 Reference and sensor's images orientation quality

Table 2 presents the photogrammetric processing and quality assessment results for four timber samples and all associated camera positions based on close-range images. It includes key metrics such as the number of images used, the number of tie points generated, and the number of control and check points. Additionally, the table reports the root mean square error (RMSE) for reprojection in pixels and spatial accuracy (in millimetres) for control and check points along the X, Y, and Z axes. These metrics provide a quantitative assessment of 3D reconstruction and alignment accuracy.

The table 2 comprehensively evaluates the photogrammetric workflow applied to timber surfaces. The RMSE reprojection error, consistently low across all samples (ranging from 1.3 to 1.7 pixels), indicates robust image alignment and projection accuracy. However, the RMSE values for control and check points highlight variations in spatial accuracy, particularly along the Z-axis. For instance, timber 4 exhibits the highest RMSE on check points (13.2 mm in X, 12.9 mm in Y, and 6.5 mm in Z), suggesting potential challenges in depth accuracy for this sample. Conversely, timber 3 achieves lower RMSE values, particularly for control points along the Z-axis (1.1 mm), indicating superior reconstruction precision.

The number of tie points also plays a crucial role in reconstruction accuracy, with higher tie point counts (e.g., 227,959 for timber 2) generally contributing to improved image connectivity but not necessarily translating to uniform spatial accuracy. These discrepancies underscore the importance of balancing image quantity, tie point density, and quality control to achieve optimal results in the 3D reconstructing timber surfaces.

### 3.2 Sensor position determination

The application of the algorithm for determining the position of the sensor relative to the reference timber face enabled the determination of geometric relationships. It facilitated the analysis of local geometric variations based on the points used to define the reference plane on the timber. These variations were utilised to correct the EM signal. Figure 6 illustrates an example of the sensor's placement relative to the timber and the deviation between points and the best-fitting plane.

### 3.3 The quality assessment of different measurement techniques utilised for the 3D shape of timber determination

As previously mentioned, the position of an EM sensor is photogrammetrically recorded with a beam context during the data acquisition to localise an EM device in the 3D model and create a correlation between internal and external structures (Fig. 6). Therefore, it is crucial to generate a high-quality, accurate 3D model and consequently define, which digitisation method is most appropriate, namely photogrammetry (based on a digital camera), iPhone-based recording combining photogrammetry with LiDAR or classic TLS, as well as matching method provides higher data quality for generating photogrammetric 3D models.

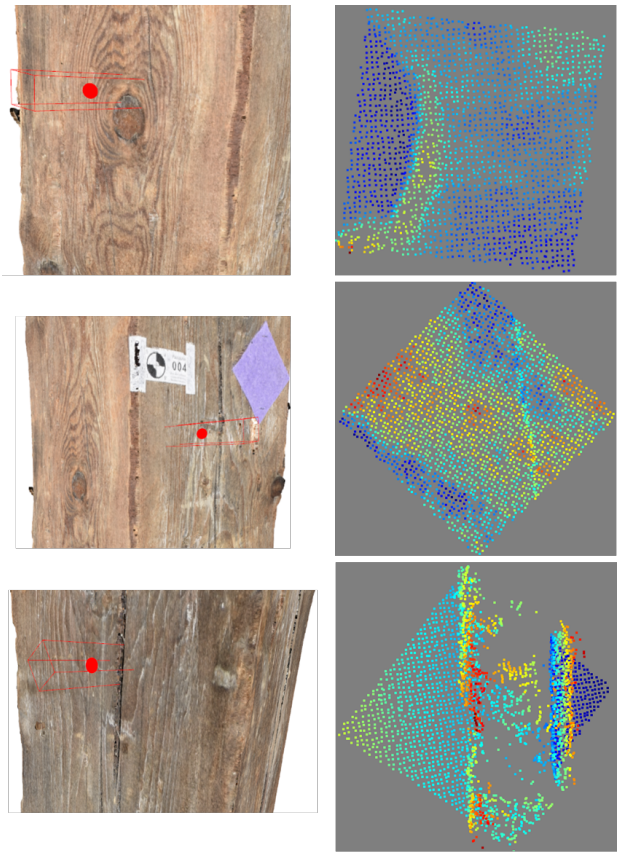

a b

Figure 6. Examples of (a) orientation of the sensor (red dot and red bounding box) to the timber and (b) map of distances between the best-fitted plan and each point.

The quality analysis of 3D point clouds from different acquisition sources and matching methods has been carried out to answer these questions. For this purpose, the point cloud of a beam was taken as an example, where EM sensor acquisition was performed in combination with photogrammetric recording. This beam has a relatively large crack on one side, which runs along its length, and several finer features, such as knots and processing marks (Fig. 7).

Figure 7. Examples of the real surface structure of historic timber with cracks, wooden knots and processing marks.

Comparing results from PBA3 (Number of Views is 2) and PBA7 (Number of Views is 8), only slight differences can be noticed. For example, the standard deviation for the Normal change rate in PBA7 is approximately lower than in PBA3 (with the same local neighbourhood radius), which provides more distinct characteristics (e.g. cracks, Fig. 8b) and is more robust to noise.

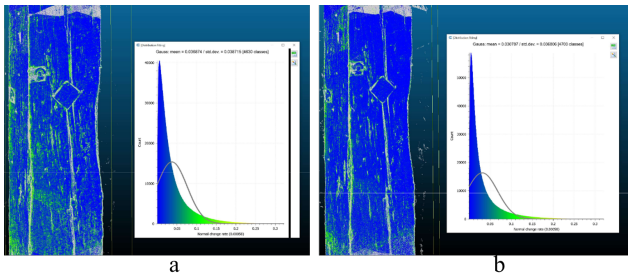

a b

Figure 8. The normal change rate results of (a) PBA3 and (b) PBA7 - show more accurate surface data and clearly defined features by PBA7.

Roughness analysis also shows that the results of PBA7 demonstrate more evident wood surface structures. In contrast, the results of PBA3 are somewhat susceptible to noise (especially annual rings, Fig. 9b). The Density test also showed higher results with PBA7, while the planarity test had less visible effects.

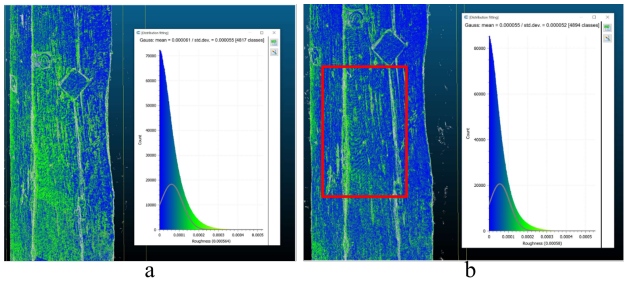

a b

Figure 9. The roughness analysis results of (a) PBA3 and (b) PBA7 - show more evident annual ring structure by PBA7.

The same analysis principles were used for the semi-global-matching method (SGM 1-6; Fig. 10). Therefore, the matching model with view 8 (SGM1) numbers performed better than the matching model with view 2 (SGM6) numbers. Thus, figure 10 shows the normal change rate and roughness analysis results, demonstrating better visual recognisability of the wood surface structure in SGM1, which also has a higher point cloud density.

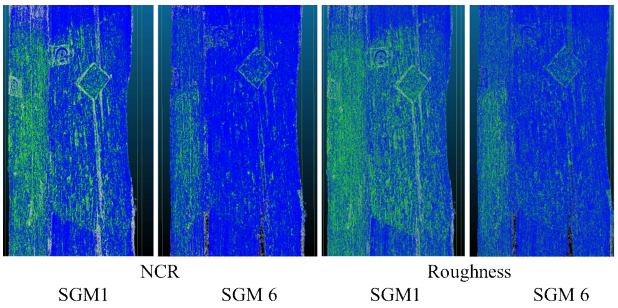


Figure 10. NCR and roughness analysis results for SGM 1 and SGM 6.

In PBA 7, a more detailed 3D reconstruction provides a reasonably accurate representation of the surface features (e.g., annual rings). Subsequently, the terrestrial laser scanner and iPhone data were analysed similarly. The timber point cloud from the TLS shows evenly distributed planarity, roughness, normal change rate and relatively low surface density (Fig. 11), indicating insufficient surface detail reconstruction from one side and relatively low informative value from another. In addition, this model has relatively many artefacts on the beam edges. The data captured with iPhone could be exported as e57 point clouds and internally processed mesh models in obj format. Although the mesh model demonstrates photorealistic textures, the model cannot be estimated geometrically. The point cloud suitable for analysis is relatively sparse (density values are lower than TLS point clouds) but shows more details (e.g. cracks concerning roughness and normal change rate), which amount, however, is not very meaningful. Nevertheless, the point cloud itself has almost no artefacts on edges.

## 4. Discussion

The analysis of geometric features was conducted across various datasets, focusing on planarity, roughness, surface density, and normal change rate. The number of views varied across the datasets, ranging from 2 to 8. This comprehensive analysis of the geometric features highlights significant differences between datasets, reflecting variations in data

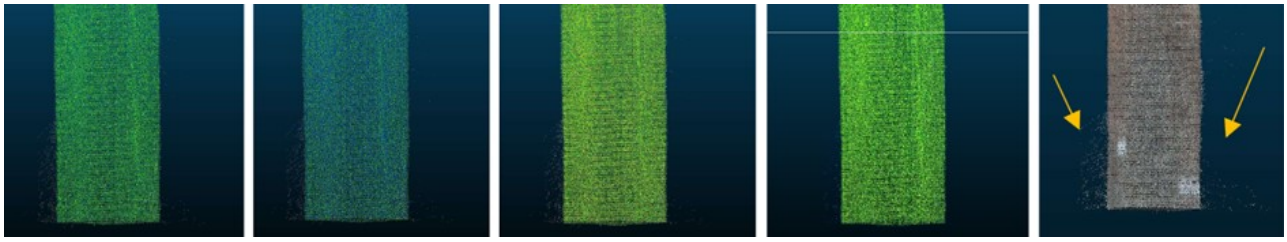

Figure 11. Geometric and radiometric feature analysis on TLS point cloud (yellow pillars show the point clouds - artefacts).

| Geometric features | Photogrammetry | | | | | | | | | | | | | iPhone | BLK |
|---|---|---|---|---|---|---|---|---|---|---|---|---|---|---|---|
| | PBA 1 | PBA 2 | PBA 3 | PBA 4 | PBA 5 | PBA 6 | PBA 7 | SGM 1 | SGM 2 | SGM 3 | SGM 4 | SGM 5 | SGM 6 | | |
| Number of views | 4 | 3 | 2 | 5 | 6 | 7 | 8 | 8 | 6 | 5 | 4 | 3 | 2 | | |
| Planarity | | | | | | | | | | | | | | | |
| Gauss mean | 0.61 | 0.59 | 0.59 | 0.62 | 0.61 | 0.62 | 0.62 | 0.58 | 0.58 | 0.58 | 0.59 | 0.60 | 0.64 | 0.58 | 0.28 |
| Std.dev. | 0.19 | 0.19 | 0.19 | 0.19 | 0.19 | 0.19 | 0.19 | 0.19 | 0.19 | 0.19 | 0.19 | 0.19 | 0.18 | 0.19 | 0.15 |
| Roughness | | | | | | | | | | | | | | | |
| Gauss mean | $5 * 10^{-5}$ | $5.9 * 10^{-5}$ | $6.1 * 10^{-5}$ | $5.7 * 10^{-5}$ | $5.6 * 10^{-5}$ | $5.6 * 10^{-5}$ | $5.5 * 10^{-5}$ | $7 * 10^{-5}$ | $7 * 10^{-5}$ | $7 * 10^{-5}$ | $6.9 * 10^{-5}$ | $6.7 * 10^{-5}$ | $5.9 * 10^{-5}$ | $37.7 * 10^{-5}$ | $106 * 10^{-5}$ |
| Std.dev. | $5* 10^{-5}$ | $5.3* 10^{-5}$ | $5.5* 10^{-5}$ | $5.3* 10^{-5}$ | $5.2* 10^{-5}$ | $5.3* 10^{-5}$ | $5.2* 10^{-5}$ | $6.3* 10^{-5}$ | $6.3* 10^{-5}$ | $6.3* 10^{-5}$ | $6.3* 10^{-5}$ | $6.2* 10^{-5}$ | $5.8* 10^{-5}$ | $60* 10^{-5}$ | $80* 10^{-5}$ |
| Surface density | | | | | | | | | | | | | | | |
| Gauss mean | $152.6 * 10^{5}$ | $151.3 * 10^{5}$ | $150.6 * 10^{5}$ | $153.4 * 10^{5}$ | $153.3 * 10^{5}$ | $153.7 * 10^{5}$ | $153.9 * 10^{5}$ | $120.3 * 10^{5}$ | $119.5 * 10^{5}$ | $118.3 * 10^{5}$ | $115.9 * 10^{5}$ | $110.4 * 10^{5}$ | $95.6 * 10^{5}$ | $0.12 * 10^{5}$ | $0.83 * 10^{5}$ |
| Std.dev. | $66.9 * 10^{5}$ | $66.7 * 10^{5}$ | $66.8 * 10^{5}$ | $67.5 * 10^{5}$ | $67.7 * 10^{5}$ | $67.6 * 10^{5}$ | $67.7 * 10^{5}$ | $58.2 * 10^{5}$ | $58.3 * 10^{5}$ | $57.7 * 10^{5}$ | $57 * 10^{5}$ | $53.9 * 10^{5}$ | $45 * 10^{5}$ | $0.03 * 10^{5}$ | $0.22 * 10^{5}$ |
| Normal change rate | | | | | | | | | | | | | | | |
| Gauss mean | $33.6 * 10^{-3}$ | $36 * 10^{-3}$ | $37.6 * 10^{-3}$ | $32.5 * 10^{-3}$ | $32.2 * 10^{-3}$ | $31.6 * 10^{-3}$ | $30.8 * 10^{-3}$ | $44.4 * 10^{-3}$ | $43.9 * 10^{-3}$ | $42.9 * 10^{-3}$ | $41.5 * 10^{-3}$ | $35.9 * 10^{-3}$ | $21.4 * 10^{-3}$ | $4.2 * 10^{-3}$ | $170 * 10^{-3}$ |
| Std.dev. | $37.8 * 10^{-3}$ | $38.8 * 10^{-3}$ | $38.9 * 10^{-3}$ | $37.4 * 10^{-3}$ | $37.2 * 10^{-3}$ | $37.2 * 10^{-3}$ | $36.8 * 10^{-3}$ | $44.6 * 10^{-3}$ | $44.3 * 10^{-3}$ | $43.5 * 10^{-3}$ | $42.8 * 10^{-3}$ | $39.3 * 10^{-3}$ | $27.9 * 10^{-3}$ | $12 * 10^{-3}$ | $54 * 10^{-3}$ |

Table 3. The analysis results on different reconstruction techniques and digitalisation methods (for units explanation s. chap. 2.3).

quality and measurement conditions across different methods such as photogrammetry, iPhone, and BLK (Tab. 3).

Based on the analysis of the geometric features, the photogrammetric approach using the patch-based matching algorithm with (PBA7) as well as semi-global matching (SGM1) with Number of Views 8 in both cases appears to be the most suitable for surface reconstruction. It should also be noted that the Number of Views was the decisive parameter for a finer detailing of the reconstructed surface. Comparing PBA and SGM results (namely PBA7 vs SGM 1), it can be noticed that PBA has considerably higher detail reconstruction of the wood surface structures in contrast to the SGM model, which is crucial for localisation of the EM sensor as well as mapping of external wood features. On the other hand, the PBA model has more outliers, although this can be filtered automatically using, e.g. statistical outlier filter (SOR). An important point is that a detailed surface reconstruction i) contains meaningful information about wood condition and ii) is crucial for future fusion with internal wood structures.

The BLK method consistently shows higher Gauss mean values for planarity (0.646) and lower standard deviations, indicating less detailed and precise results. The roughness values are low, indicating a smooth and less detailed surface, which is essential for precise 3D modelling and representation. Additionally, the surface density is lower compared to other techniques, which may not guarantee adequate surface detail.

The iPhone-based recording provides a photorealistic mesh model with minimal noise. However, the generated 3D point cloud demonstrates only slightly better resolution compared to the laser scanning data but is still not detailed enough compared to the classic photogrammetric approach. However, when considering the costs of using an iPhone in comparison to other methods (e.g. laser scanning, which requires expensive equipment, specialised software, and trained personnel), the results are of sufficient quality to effectively localise EMS sensors. The analysis results can be seen in Table 3.

## 5. Conclusions

The current study investigates alternative non-invasive methods for analysing the condition of historic timber structures, specifically focusing on electromagnetic sensing. The key objective is to accurately localise EMS measuring devices within beams. By combining EM sensor with photogrammetry and laser scanning, the research highlights the potential for accurate, detailed timber analysis without the need for invasive methods, offering significant benefits for cultural heritage preservation. The results indicate that while methods such as photogrammetry (also in combination with LiDAR) and TLS each have unique advantages, the combination of dense point clouds and high-resolution 3D models significantly enhances the accuracy of timber evaluations. Moreover, the georeferencing process, aided by photogrammetry and computational algorithms, proves crucial in improving sensor data's localisation and spatial alignment. The findings suggest that integrating these technologies can facilitate a more reliable and resource-efficient approach to timber conservation, ensuring the long-term preservation of heritage wooden structures while minimising unnecessary resource consumption.

The further development of this technique involves the fusion and comprehensive interpretation of EM and optical data using artificial intelligence (AI) and machine learning alongside image and signal processing methods. In this context, we will investigate how the internal structures captured by EM sensor correlate with external surface information (e.g. detected cracks, insect affection, wood knots).

## Acknowledgements

This project was funded by internal research support of the Centre for Heritage Conservation Studies and Technologies/ University of Bamberg (Germany).

**References**

Amsters, R., Demeester, E., Stevens, N., Lauwers, Q., Slaets, P., 2019. Evaluation of Low-Cost/High-Accuracy Indoor Positioning Systems, ALLSENSORS 2019: Proceedings of the Fourth International Conference on Advances in Sensors. Actuators. Metering and Sensing. IARIA XPS - Xpert Publishing Services, Athens, 15–22.

Bianco, S., Ciocca, G., & Marelli, D., 2018: Evaluating the Performance of Structure from Motion Pipelines. *Journal of Imaging*, *4*(8), 98. https://doi.org/10.3390/jimaging4080098

Börlin, N., Murtiyoso, A., Grussenmeyer, P., Menna, F., Nocerino, E., 2018. Modular bundle adjustment for photogrammetric computations. *Int. Arch. Photogramm. Remote Sens. Spatial Inf. Sci.,* XLII–2, 133–140.

Ebner, F., 2018. Festigkeitsuntersuchungen an verbauten Konstruktionshölzern (Unpublished Master’s thesis). Otto-Friedrich University Bamberg, Bamberg.

Erler, K., 2004: *Alte Holzbauwerke Beurteilen und Sanieren*. Huss-Medien GmbH Verl. für Bauwesen, Berlin.

Gkantou, M., Muradov, M., Kamaris, G., Hashim, D., Atherton, W., Kot, P., 2019. Novel Electromagnetic Sensors Embedded in Reinforced Concrete Beams for Crack Detection. *Sensors* 19, 1–14. https://doi.org/10.3390/s19235175

Hansmann, C., Huber, C., Teischinger, A., 2018. Technology Road Map for Hardwood in Lower Austria. 8th Hardwood conference - new aspects of hardwood utilization - from science to technology Sopron, 2018, 172-174.

Ijaz, F., Yang, H., Ahmad, A.W., Lee, C., 2013. Indoor positioning: A review of indoor ultrasonic positioning systems. 15th International Conference on Advanced Communications Technology (ICACT), 1146–1150.

Kersten, T., Lindstaedt, M., 2022. Geometric accuracy investigations of terrestrial laser scanner systems in the laboratory and in the field. Applied Geomatics 14, 421–434.

Kot, P., Muradov, M., Gkantou, M., Kamaris, G., Hashim, D., Yeboah, D., 2021. Recent Advancements in Non-Destructive Testing Techniques for Structural Health Monitoring. Applied Sciences 11, 1–28. https://doi.org/10.3390/app11062750

Kot, P., Shaw, A., Riley, M., Ali, A., Cotgrave, A., 2016. The Feasibility of Using Electromagnetic Waves in Determining Membrane Failure Through Concrete. International Journal of Civil Engineering 15.

Li, J., Han, G., Zhu, C., Sun, G., 2016. An Indoor Ultrasonic Positioning System Based on TOA for Internet of Things. Mobile Information Systems 2016, 1–10.

Li, X., Li, Y., Xie, X., Xu, L., 2018. Lab-built terrestrial laser scanner self-calibration using mounting angle error correction. Opt Express 26, 14444.

Linke, G., 2024. Festigkeitssortierung von Holzbauteilen beim Bauen im Bestand : ein Beitrag zur substanzschonenden Erhaltung historischer Gebäude (Dissertation). BTU Cottbus - Senftenberg, Cottbus. https://doi.org/10.26127/BTUOpen-6690

Linke, G., Rug, W., Pasternak, H., 2017. Festigkeitssortierung von Bauholz in historischen Gebäuden - Bericht zum Stand der Technik. Bauingenieur 92, 229–236.

Markiewicz, J., Łapiński, S., Kot, P., Tobiasz, A., Muradov, M., Nikel, J., Shaw, A., Al-Shamma, A., 2020. The Quality Assessment of Different Geolocalisation Methods for a Sensor System to Monitor Structural Health of Monumental Objects. Sensors 20, 1–39. https://doi.org/10.3390/s20102915

Mautz, R., 2012. Indoor Positioning Technologies. ETH, Zurich. https://doi.org/10.3929/ethz-a-007313554

Medic, T., Kuhlmann, H., Holst, C., 2019: Automatic in-situ self-calibration of a panoramic TLS from a single station using 2D keypoints, *ISPRS Ann. Photogramm. Remote Sens. Spatial Inf. Sci.,* IV-2/W5, 413–420.

Muradov, M., Kot, P., Markiewicz, J., Łapiński, S., Tobiasz, A., Onisk, K., Shaw, A., Hashim, D., Zawieska, D., Mohi-Ud-Din, G., 2022. Non-destructive system for in-wall moisture assessment of cultural heritage buildings. Measurement 203.

NumPy, 2024. The fundamental package for scientific computing with Python. https://numpy.org/.

Nyimbili, P., Demirel, H., Seker, D., Erden, T., 2016. Structure from Motion (SfM) - Approaches and Applications, in: Proceedings of the International Scientific Conference on Applied Sciences. Antalya.

Open3D, 2024. Modern Library for 3D Data Processing. https://www.open3d.org/.

Puertolas-Montañez, J., Mendoza-Rodriguez, A., Sanz-Prieto, I., 2013: Smart Indoor Positioning/Location and Navigation: A Lightweight Approach. *International Jorunal of Interactive Multimedia and Artificial Intelligence,* 2 (2), 43–50.

Rinn, F., 2016. Intact-decay transitions in profiles of density-calibratable resistance drilling devices using long thin needles. Arboric J 38, 1–14.

Rug, W., Held, H., 1995. Die Bohrwiderstandsmessung (Teil 1,2): Zerstörungsarme Untersuchung alter Holzkonstruktionen. Bau-Zeitung 4, 50–59.

Tan, K., Cheng, X., 2016. Correction of Incidence Angle and Distance Effects on TLS Intensity Data Based on Reference Targets. Remote Sens (Basel) 8, 251.

Teunissen, P., 2024. Adjustment theory: an introduction. TU Delft OPEN Publishing. https://doi.org/10.59490/tb.95

Xu, H., Wu, M., Li, P., Zhu, F., Wang, R., 2018. An RFID Indoor Positioning Algorithm Based on Support Vector Regression. Sensors 18, 1504.

Zafari, F., Gkelias, A., Leung, K., 2017. A Survey of Indoor Localization Systems and Technologies. IEEE Communications Surveys & Tutorials PP.